JCI insight

RESEARCH ARTICLE

Activity of $Na_V1.2$ promotes neurodegeneration in an animal model of multiple sclerosis

Benjamin Schattling,[1] Walid Fazeli,[2,3,4] Birgit Engeland,[2,3] Yuanyuan Liu,[5] Holger Lerche,[5] Dirk Isbrandt,[2,3] and Manuel A. Friese[1]

[1]Institut für Neuroimmunologie und Multiple Sklerose, Universitätsklinikum Hamburg-Eppendorf, Hamburg, Germany. [2]Institut für Molekulare und Verhaltensneurowissenschaften, Universität zu Köln, Köln, Germany. [3]Deutsches Zentrum für Neurodegenerative Erkrankungen, Bonn, Germany. [4]Klinik für Kinder- und Jugendmedizin, Uniklinik Köln, Köln, Germany. [5]Abteilung Neurologie mit Schwerpunkt Epileptologie, Hertie-Institut für klinische Hirnforschung, Universitätsklinikum Tübingen, Tübingen, Germany.

Counteracting the progressive neurological disability caused by neuronal and axonal loss is the major unmet clinical need in multiple sclerosis therapy. However, the mechanisms underlying irreversible neuroaxonal degeneration in multiple sclerosis and its animal model experimental autoimmune encephalomyelitis (EAE) are not well understood. A long-standing hypothesis holds that the distribution of voltage-gated sodium channels along demyelinated axons contributes to neurodegeneration by increasing neuroaxonal sodium influx and energy demand during CNS inflammation. Here, we tested this hypothesis in vivo by inserting a human gain-of-function mutation in the mouse $Na_V1.2$-encoding gene *Scn2a* that is known to increase $Na_V1.2$-mediated persistent sodium currents. In mutant mice, CNS inflammation during EAE leads to elevated neuroaxonal degeneration and increased disability and lethality compared with wild-type littermate controls. Importantly, immune cell infiltrates were not different between mutant EAE mice and wild-type EAE mice. Thus, this study shows that increased neuronal $Na_V1.2$ activity exacerbates inflammation-induced neurodegeneration irrespective of immune cell alterations and identifies $Na_V1.2$ as a promising neuroprotective drug target in multiple sclerosis.

Introduction

Multiple sclerosis is an inflammatory demyelinating disease that currently affects over 2 million individuals worldwide, making it the most common cause for nontraumatic neurological disability in young adults. The extent of neuronal and axonal degeneration is best correlated with irreversible disability in multiple sclerosis patients and therefore their long-term outcome and quality of life. While acute exacerbations in multiple sclerosis patients are thought to reflect bouts of inflammatory activity that are suppressed by immunomodulatory drugs, the mechanisms underlying progressive neurodegeneration in multiple sclerosis and its animal model, experimental autoimmune encephalomyelitis (EAE), remain unresolved (1). As a consequence, there are currently no therapies available that counteract progression of neurological disability caused by neuronal and axonal loss, which is the largest unmet clinical need in multiple sclerosis therapy.

Dysregulated neural ion channels have been proposed to drive neuroaxonal injury during CNS inflammation and might therefore represent promising neuroprotective drug targets (2–4). In unmyelinated axons, voltage-gated sodium channels (VGSC) are evenly distributed along the entire axolemma. By contrast, myelinated axons are characterized by a high density of VGSC at nodes of Ranvier, which allows accelerated saltatory action potential conduction. During brain maturation, a switch in VGSC isoform expression accompanies progressive myelination of axons. Unmyelinated axons and immature nodes of Ranvier show high densities of $Na_V1.2$ (encoded by *SCN2A*), whereas mature nodes of Ranvier in myelinated axons express high densities of $Na_V1.6$ (encoded by *SCN8A*) (5). However, these physiological developmental changes of VGSC isoform usage are dysregulated in demyelinated areas during multiple sclerosis and EAE. Loss of myelin results in a reexpression of $Na_V1.2$, which is — together with $Na_V1.6$ — distributed along the entire denuded axolemma (6, 7). Presumably, this upregulation initially counteracts myelin loss and pre-

Authorship note: B. Schattling and W. Fazeli are co–first authors and contributed equally to this work. D. Isbrandt and M.A. Friese are co-senior authors and contributed equally to this work.

Conflict of interest: The authors have declared that no conflict of interest exists.

Submitted: July 29, 2016
Accepted: October 18, 2016
Published: November 17, 2016

Reference information:
JCI Insight. 2016;1(19):e89810.
doi:10.1172/jci.insight.89810.

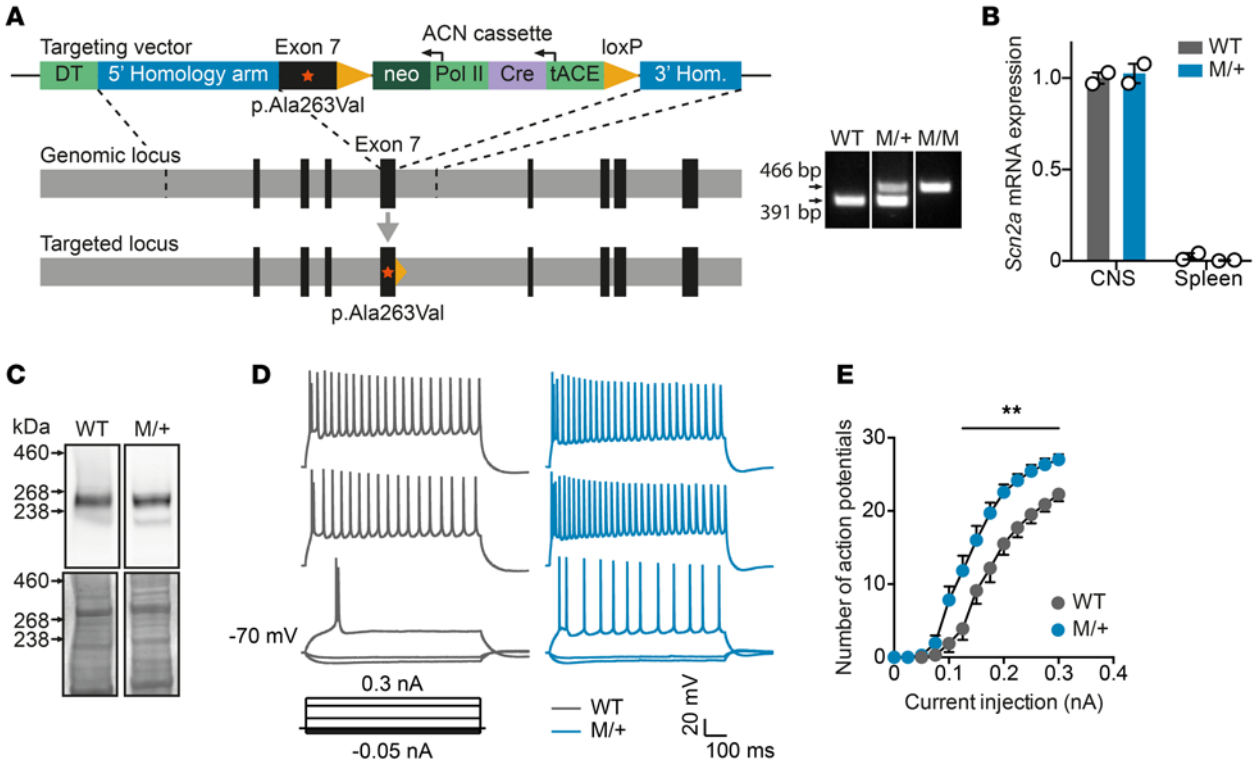

Figure 1. Generation and characterization of *Scn2a*^{A263V} channelopathy mice. (**A**) Scheme of the targeting strategy of knockin mice carrying the human *p.Ala263Val* gain-of-function mutation in the *Scn2a* gene (left), and a representative image of PCR genotyping of wild-type, heterozygous (M/+), and homozygous (M/M) knockin animals (right). The lanes are from the same gel but were noncontiguous. (**B**) Quantitative real-time PCR of mouse *Scn2a* transcripts normalized to *TATA-box-binding protein* transcripts from wild-type and M/+ mutant whole spinal cord (n = 2 per group) or whole spleen homogenates (n = 2 per group). ΔCT values were arbitrarily calibrated to CNS cDNA of wild-type mice as the standard value of 1. Data are shown as mean ± SEM. (**C**) Western blot of cortical cell membranes from wild-type and M/+ mice at 3 weeks of age, demonstrating comparable abundance of $Na_V1.2$ protein. The lanes are from the same gel but were noncontiguous. (**D**) Representative traces of current-clamp recordings from P10 to P12 hippocampal CA1 pyramidal neurons of wild-type and M/+ mice (injected currents from bottom to top trace in nA: −0.05; −0.025; 0.1; 0.225; 0.3). (**E**) Number of evoked action potentials plotted against the injected current. Wild-type: n = 10 cells from 2 animals; M/+: n = 15 cells from 3 animals. Data are shown as mean ± SEM.; 2-way analysis of variance (P = 0.0037 for genotype effect) was used for statistical analysis; $^{**}P < 0.01$.

serves action potential conduction (8, 9), while persistent changes might be maladaptive and lead to axonal degeneration via a proposed cascade of intraaxonal sodium accumulation, subsequent axonal energy deprivation, axonal swelling, and calcium overload (3).

In line with this proposed mechanism, sodium imaging of multiple sclerosis patients' brains by 7 Tesla magnetic resonance imaging revealed that the intracellular sodium concentration within gray and white matter was increased compared with healthy controls and that increased intracellular sodium concentrations correlated with disease duration and degree of clinical disability (10, 11). Moreover, the relevance of neuroaxonal sodium homeostasis in inflammatory neurodegeneration is supported by circumstantial evidence in EAE studies indicating that treatment with nonselective VGSC blockers can improve the clinical course (12–14). However, since these blockers also substantially dampen the immune response (15, 16), the mechanisms underlying the beneficial effects of VGSC blockers in EAE have not been unraveled. In particular, it remains unclear whether and how specific subtypes of VGSC contribute to neurodegeneration.

For more than a decade, a prevailing hypothesis in the field of inflammatory neurodegeneration holds that neuronal reexpression and axonal distribution of VGSC directly contribute to axonal degeneration in multiple sclerosis and EAE. Of the two predominant sodium channel isoforms at axonal membranes in the CNS, $Na_V1.6$ was thought to be the main driver of axonal injury, since $Na_V1.2$ produces a smaller persistent current than $Na_V1.6$ (17). However, it has so far not been possible to provide direct in vivo evidence for the contribution of persistent sodium influx in neuroaxonal degeneration during CNS inflammation and the relative contribution of the two isoforms, as complete loss of $Na_V1.6$ (18) or $Na_V1.2$ (19) function results in perinatal death of mice. To circumvent this problem, we generated a mouse model with genetically

increased $Na_V1.2$ activity and examined the contribution of persistent neuroaxonal sodium influx mediated by $Na_V1.2$ to neuroaxonal degeneration in EAE. Our results demonstrate that increased neuroaxonal $Na_V1.2$ activity promotes neurodegeneration without affecting immune cell responses.

Results

Generation of Scn2a^{A263V} mutant mice. To address the unresolved question of whether increased neuronal sodium influx contributes to inflammation-induced axonal injury, we generated a genetic mouse model of $Na_V1.2$ channelopathy by inserting a human $Na_V1.2$ gain-of-function mutation into the *Scn2a* gene locus (*Scn2a^{A263V}*; Figure 1A). This mutation, which was previously shown to result in an increased tetrodotoxin-sensitive persistent sodium current (20), did not affect either $Na_V1.2$ mRNA expression or protein levels in brains from heterozygous mice (Figure 1, B and C). Current-clamp recordings in acute hippocampal slices revealed increased excitability of CA1 pyramidal neurons from heterozygous *Scn2a$^{A263V/+}$* mutant (M/+) mice as compared to neurons from wild-type littermate controls at P10–12 (Figure 1, D and E), a developmental period during which $Na_V1.2$ is known to be expressed by these cells (21). In contrast to homozygous mutant mice, which showed frequent epileptic seizures associated with an impaired survival rate (data not shown), M/+ mice did not exhibit an overt behavioral phenotype or increased mortality and were therefore exclusively used for comparison to wild-type littermates in our EAE experiments.

Scn2a^{A263V} gain-of-function mutation exacerbates EAE without changes in the immune response. To identify whether $Na_V1.2$ activity contributes to neurodegeneration during chronic CNS inflammation, we challenged heterozygous *Scn2a$^{A263V/+}$* mutant mice and their wild-type littermates by inducing EAE. As we observed a thus far unexplored sex difference in disease severity, with male mutant mice showing a more severe EAE disease course — only 4 of 11 animals survived 4 weeks after immunization (Figure 2A and Table 1) — all further EAE experiments were carried out with female mice. Strikingly, female mutant mice showed exacerbated clinical disability, with a disease onset similar to that of wild-type mice, but a severely impaired disease remission (Figure 2B and Table 1). This was paralleled by an impaired recovery from body weight loss (Figure 2C and Table 1). Notably, there was no difference in the extent of inflammatory lesions (Figure 2D), demyelination (Figure 2E), or astrocytic activation (Figure 2F) in spinal cords from M/+ and wild-type mice at the peak of disease (14 days after immunization) or chronic phase of disease (30 days after immunization). Further, the *Scn2a$^{A263V/+}$* mutation did not have an effect on priming of lymph node–isolated $MOG_{35–55}$-specific T cells measured 7 days after immunization (Figure 2G) or on the total number of CNS-infiltrating $CD45^+$ leukocytes (Figure 2H) or on subset composition of CNS immune cell infiltrates at day 15 after immunization (Figure 2I).

Enhanced neuroaxonal $Na_V1.2$ activity increases axonal injury and energy consumption during EAE. Finally, to investigate whether the observed difference in EAE disease course can be attributed to a $Na_V1.2$ activity–induced exacerbated neuroaxonal injury in mutant mice, we recorded axonal densities and energy consumption in the spinal cord. Indeed, we detected an elevated amount of amyloid precursor protein–positive (App-positive) axons, as a measure of acute axonopathy at 14 days after immunization (Figure 3A), and a reduced number of preserved axons in the dorsal column 30 days after immunization in mutant mice compared with wild-type littermates (Figure 3B). This finding was corroborated by an overall increase in hexokinase-1 expression, as a measure of neuronal glucose or energy consumption (22), in inflamed spinal cord sections of M/+ mice in comparison with wild-type controls 30 days after immunization (Figure 3C).

Discussion

Here, we show that the activity of the neuronal sodium channel $Na_V1.2$ strongly influences the extent of axonal degeneration, clinical disability, and neuronal energy demand in an animal model of multiple sclerosis. Of note, the immune response was not affected by the mutation, implying that, in this model, blocking $Na_V1.2$ activity is a bona fide mechanism of neuroprotection in CNS inflammation, irrespective of immunomodulation.

To date, it is unclear whether the beneficial effects of unselective VGSC blockers in multiple sclerosis and EAE are due to an immunomodulatory or a direct axonal effect or a combination of both. We addressed this timely debate by using a mouse model of genetically increased $Na_V1.2$ activity. Based on our data, we propose that increased $Na_V1.2$ activity substantially promotes neurodegeneration in multiple sclerosis and EAE via a direct axonal mechanism, i.e., by increasing intracellular sodium concentration, which then induces a cascade of axonal degeneration, as has been proposed for $Na_V1.6$ (3, 23, 24). In fact, $Na_V1.6$ could play an even more pronounced role during inflammation-induced axonal degeneration, as it pro-

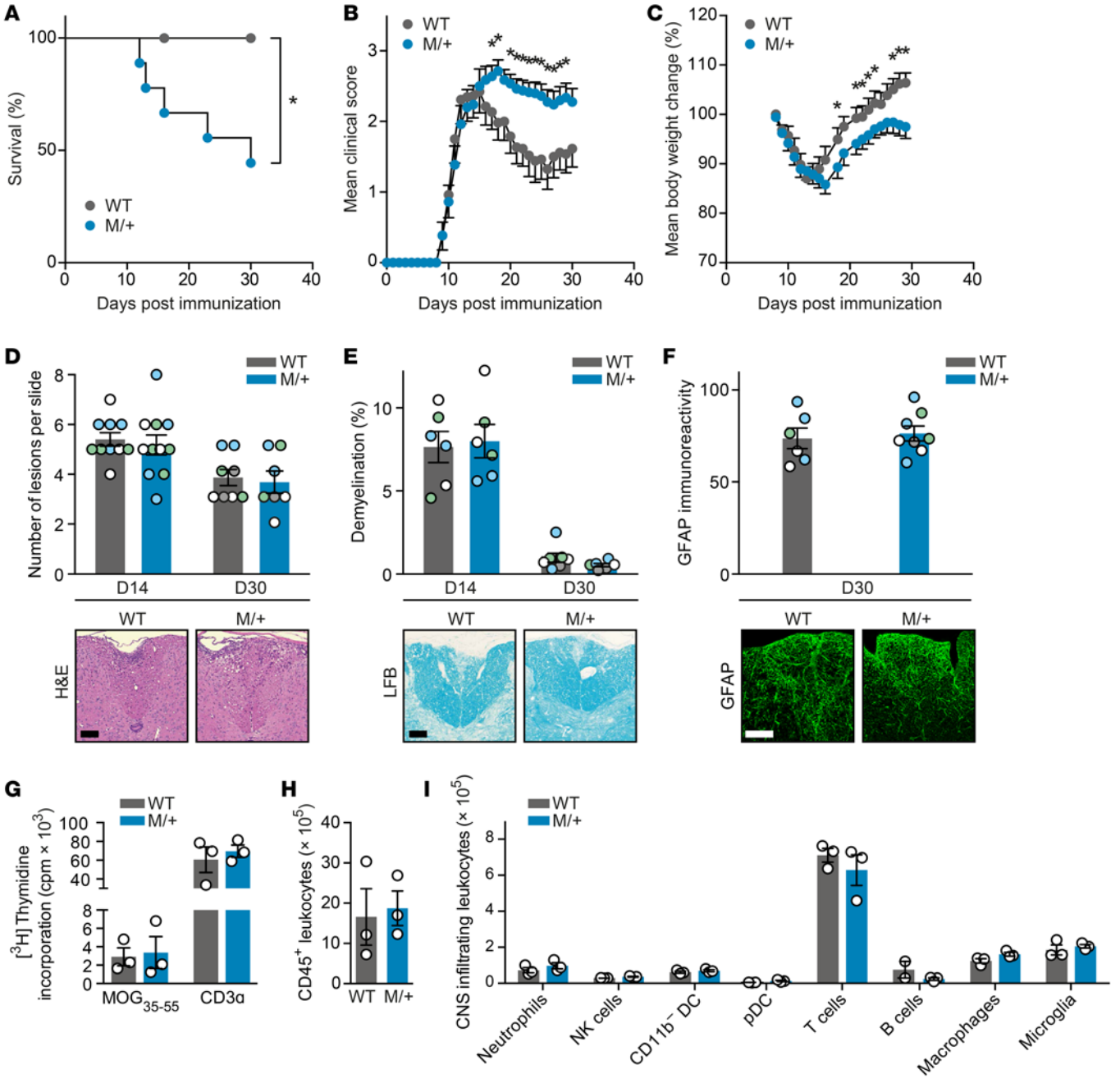

Figure 2. Heterozygous *Scn2a*^{A263V} mutation (M/+) leads to an exacerbated EAE disease course without altering immune responses. (**A**) Kaplan-Meier survival analysis of male EAE mice after immunization with MOG_{35-55} (wild-type: $n = 9$; M/+: $n = 11$; $P = 0.02$). (**B**) Clinical disability scores and (**C**) body weight changes of female EAE mice after immunization with MOG_{35-55} (wild-type: $n = 13$; M/+: $n = 20$; two independent experiments). (**D**–**F**) Representative histopathological stainings and quantifications of whole cervical spinal cord sections (**D**) or dorsal columns (**E** and **F**) of diseased mice 14 days (D14) or 30 days (D30) after immunization ($n = 3$–4 mice per group with 2–4 color-coded slices per animal). Sections were stained for cellular infiltration (**D**; H&E, sample images from D14), myelin (**E**; Luxol fast blue [LFB], sample images from D14), and astrocytes (**F**; glial fibrillary acidic protein [GFAP]). For each quantification, multiple replicates of data from individual animals were color coded (**D**–**F**). Scale bar: 100 μm. (**G**) Single-cell suspensions of draining lymph nodes were prepared 7 days after immunization from wild-type EAE ($n = 3$) and M/+ EAE ($n = 3$) mice, and restimulated with MOG_{35-55} peptide. T cell proliferation was assessed by incorporation of [methyl-^{3}H]thymidine. CNS-infiltrating cells were isolated 15 days after immunization from wild-type EAE ($n = 3$) and M/+ EAE ($n = 3$) mice, and the total number of CD45$^+$ leukocytes (**H**) and the leukocyte subsets (**I**) were analyzed by multicolor flow cytometry. All data are presented as mean ± SEM. Statistical analyses were performed by Gehan-Breslow-Wilcoxon test (**A**), Mann-Whitney test (**B** and **C**), 2-way analysis of variance with Sidak's post-hoc test (**G** and **I**), or Student's *t* test (**D**–**F** and **H**); *$P < 0.05$. Color coding has to be evaluated separately for each graph, i.e., each color represents one particular animal at one specific time point for one particular parameter.

Table 1. *Scn2a* gain-of-function mutation aggravates EAE disease course

	Wild-type Female	M/+ Female	Wild-type Male	M/+ Male
Mean maximum score (SD)	3.0 (0.8)	3.2 (0.6)	3.5 (0.5)	4.0 (0.6)[A]
Euthanized (score 4)[B]	2/17	2/23	0/9	5/11[A]
Spontaneous death (score 5)[C]	1/17	0/23	1/9	2/11
Incidence	16/17	22/23	9/9	11/11
Mean day of onset (SD)	10.9 (4.7)	10.5 (2.3)	10.6 (1.6)	10.1 (1.8)

[A]Significant difference in comparison with wild-type mice of the same sex; $P < 0.05$. [B]Not included in EAE graphs shown in Figure 2, B and C. [C]Not included in EAE graphs shown in Figure 2, A–C. M/+, *Scn2a*$^{A263V/+}$ mutant heterozygous mice.

duces a larger persistent current than $Na_V1.2$ (17) and colocalizes more often with axonal injury markers (7). Therefore, comparing human mutations in transgenic mice that result in increased persistent currents in $Na_V1.6$, such as the gain-of-function mutation p.Asn1768Asp (25–27), with the herein described transgenic $Na_V1.2$ mutant could give further insight into the relative contribution of the two VGSC isoforms in EAE and multiple sclerosis. However, $Na_V1.6$ channels are more abundantly expressed and conduct larger currents than $Na_V1.2$ channels, and $Na_V1.6$ gain-of-function mutations cause spontaneous motor seizure phenotypes in their heterozygous state (25–27), which has not been observed in our $Na_V1.2$ heterozygous mutant mice. Frequent spontaneous seizures might interfere with EAE experiments, thus complicating interpretation of the data. Besides our findings, the concept that axonal sodium accumulation contributes to neurodegeneration is supported by a recent study showing that a peripheral neuropathy–associated gain-of-function mutation of the VGSC subtype $Na_V1.7$ leads to intraaxonal sodium overload, reverse activity of the sodium/calcium exchanger, and subsequent intraaxonal calcium accumulation and toxicity (28). Notably, the particularly high sensitivity of male mutant mice to neurodegeneration revealed by our experiments is reminiscent of human multiple sclerosis patient data, suggesting that men might have an accelerated neurodegenerative disease course in comparison with women (29). While the pathomechanism remains entirely unclear, this model might allow the deciphering of differences in resilience to inflammatory stressors between male and female neurons.

There is evidence that nonspecific sodium channel blockers do not only target neuroaxonal VGSC, but also show effects on VGSC expressed on astrocytes, microglia, and other immune cells (15, 30). Considering the heterogeneous roles of the different VGSC subtypes in multiple sclerosis (31, 32), our findings in context with previous studies suggest that nonselective sodium channel blockers exert their beneficial effect at least via two mechanisms, i.e., direct axonal neuroprotection (presumably via $Na_V1.6$ and $Na_V1.2$) and immunomodulation (presumably via $Na_V1.6$, $Na_V1.5$ and off-target). While $Na_V1.2$ is reexpressed and distributed along the axolemma during multiple sclerosis (7) and EAE (6), $Na_V1.2$ expression has been detected in neither microglia nor other immune cells (Figure 1B and Supplemental Figure 1; supplemental material available online with this article; doi:10.1172/jci.insight.89810DS1); it is also not upregulated in astrocytes within multiple sclerosis plaques (31), although it is expressed by scar and reactive astrocytes within chronic multiple sclerosis plaques (33). In contrast, $Na_V1.5$ is highly upregulated in astrocytes within multiple sclerosis lesions (31) and expressed in macrophages within active multiple sclerosis lesions (34), and $Na_V1.6$ expression is elevated in microglia and macrophages in multiple sclerosis and EAE (16).

In translational medicine, while a placebo-controlled clinical multiple sclerosis trial with the anticonvulsant lamotrigine failed to show clear benefits regarding neurological disability (35), a well-designed phase II trial showed that phenytoin might be neuroprotective in multiple sclerosis patients suffering from optic neuritis (36). Of note, compressive spinal cord injury is also characterized by demyelination (37), which can be rescued by treatment with nonspecific sodium channel blockers (38), indicating that our findings could have translational relevance beyond the treatment of multiple sclerosis. Thus, unraveling the contribution of the different VGSC subtypes would enable targeted therapy in multiple sclerosis and possibly other demyelinating diseases, thereby increasing therapeutic potency and reducing adverse effects (39). As the tarantula toxin phrixotoxin 3 specifically blocks $Na_V1.2$ in vitro (40), it is, in principle, possible to develop specific blockers that might be suitable for the use in humans (39). As $Na_V1.2$ is less abundantly

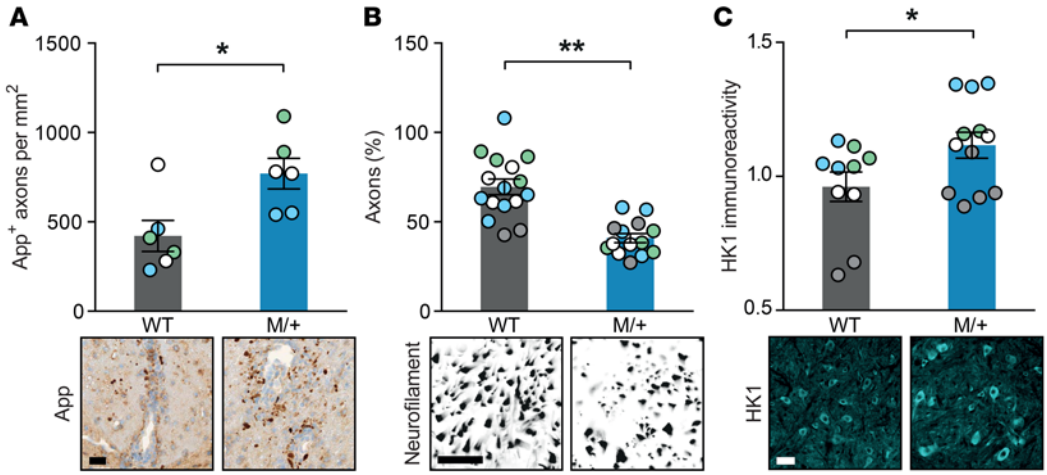

Figure 3. Enhanced $Na_V1.2$ activity results in increased axonal injury and neuronal energy consumption during EAE. Representative histopathological sections and quantification of (**A**) amyloid precursor protein (App; $P = 0.016$), (**B**) neurofilament ($P < 0.0001$), and (**C**) hexokinase-1 (HK1; $P = 0.023$) immunostainings. Dorsal columns and corticospinal tract (**A**), dorsal columns (**B**), or gray matter (**C**) of cervical spinal cord sections were stained from wild-type EAE and M/+ EAE mice 14 days (**A**; $n = 3$ mice per group with 2 color-coded slices per animal) or 30 days after immunization (**B** and **C**; $n = 4$ mice per group with 2–5 color-coded slices per animal; normalized to healthy wild-type and M/+ control mice); for each quantification, multiple replicates of data from individual animals were color coded. Scale bar: 20 μm (**A** and **C**), 2 μm (**B**). All data are presented as mean ± SEM. Statistical analyses were performed by Student's *t* test; $^*P < 0.05$, $^{**}P < 0.01$. Color-coding has to be evaluated separately for each graph, i.e., each color represents one particular animal at one specific time point for one particular parameter.

expressed than other VGSCs and shows disease-related reexpression, $Na_V1.2$-specific blockers may generate fewer unwanted side effects than $Na_V1.6$-specific blockers. Thus, our findings suggest that $Na_V1.2$ is a promising ion channel subunit to be specifically targeted in multiple sclerosis and possibly other acute and chronic CNS processes that are associated with neuroaxonal degeneration.

Methods

Animals. The *Scn2a*^{A263V} mutant knockin allele was generated by targeting of (129/Sv) ES cells with a construct containing the point mutation c.788C>T flanked by *Scn2a* genomic sequences. For selection and excision of the neo gene, an ACN cassette (41) was included in the targeting vector pKo Scrambler. The linearized targeting vector was electroporated into R1 ES cells, which were subjected to selection by geneticin (G418, Invitrogen). Homologous recombination was verified by PCR analysis. We propagated the line by backcrossing *Scn2a*$^{A263V/+}$ mutant heterozygotes to C57BL/6J wild-type mice (The Jackson Laboratory). Genotyping was performed by amplification of wild-type and mutant alleles following standard protocols. A 391-bp genomic fragment of *Scn2a* containing the mutation was amplified by PCR with the following primers: 5′-CCAAACCATGATGGGGGTTAG-3′ and 5′-GAGCTGCAGCCCTATTAATAC-3′. A 466-bp genomic fragment of Scn2a wild-type DNA was amplified with the following primers: 5′-TGTCTGAGTGTCTTTGCTCTC-3′ and 5′-GATCATGCACGTTGAAATGGC-3′. Mice were kept under specific pathogen–free conditions in the Central Animal Facility at the University Medical Center Hamburg-Eppendorf (UKE). Age-matched adult animals (10 to 20 weeks of age) were used in all experiments.

Gene expression analysis. mRNA was purified using the RNeasy Mini Kit (Qiagen) and reverse transcribed to cDNA with the RevertAid H Minus First-Strand cDNA Synthesis Kit (Fermentas) according to the manufacturer's instructions. For quantitative real-time PCR, the following TaqMan Gene Expression Assays were used: *Scn2a*, Mm01270359_m1 and *Tbp*, Mm00446971_m1. Gene expression was analyzed by real-time PCR performed in an ABI Prism 7900 HT Fast Real-Time PCR System (Applied Biosystems) using the ΔCt method for relative quantification with *Tbp* as endogenous control.

Western blot analysis. Membrane proteins were isolated from mouse cortices at P21 using the Proteo-Extract Native Membrane Protein Extraction Kit (Merck Millipore). Protein concentration was measured with the BCA assay (Thermo-Fisher). Samples containing 40 μg protein were incubated at 70°C for 10 minutes in sample loading buffer before electrophoresis on 3%–8% gradient Tris-Acetate gels (Thermo Fisher). After transfer, filters were cut and incubated with polyclonal antibody to $Na_V1.2$ (AB5206, 1:200; Millipore) in PBS containing 5% milk powder and 2% TWEEN.

Electrophysiology. Brain slices were obtained as previously described (42). Before recordings, slices were incubated in normal aCSF solution at 36°C for 1 hour for recovery. Whole-cell current clamp recordings were performed at 34°C in hippocampal CA1 pyramidal neurons with an Axopatch 200B amplifier and a DigiData1420 digitizer. Data were obtained and analyzed by pClamp 10.2 software (all Molecular Devices). Borosilicate glass pipettes had a resistance of 3–5 MΩ. The pipette solution contained (in mM): 5 KCl, 4 ATP-Mg, 10 phosphocreatine, 0.3 GTP-Na, 10 HEPES, 125 K-gluconate, 2 $MgCl_2$, and 10 EGTA, with a final pH of 7.2 and an osmolarity of 290 mOsm/kg. Cells were held at –70 mV. Signals were low-pass filtered at 30 kHz and sampled at 100 kHz.

EAE induction. Animals were immunized subcutaneously with 200 μg $MOG_{35–55}$ peptide (Schafer-N) in 50 μl complete Freund's adjuvant containing 4 mg/ml *Mycobacterium tuberculosis* (Difco); mice were injected once in the left and once in the right flank. In addition 200 ng pertussis toxin (Calbiochem) was injected intravenously on the day of immunization and 48 hours later. Mice were scored for clinical signs daily by the following system: 0, no clinical deficits; 1, tail weakness; 2, hind limb paresis; 3, partial hind limb paralysis; 3.5, full hind limb paralysis; 4, full hind limb paralysis and forelimb paresis; and 5, premorbid or dead. Animals reaching a clinical score ≥4 were euthanized. The experimenters were blinded to the genotype until the end of the experiment, including data analysis. The animals were delivered to the experimenters separated by litters; each animal was numbered in chronological order independent of the genotype. For female mice, two independent sets of EAE experiments were conducted. The data were pooled for final data analysis. In contrast, due to the substantially impaired survival rate of male mutant mice challenged by EAE and the subsequent ethical considerations, we did not repeat the experiment with male mice. In the first round of experiments, we used mice from the third generation of backcrossing with C57BL/6. In the second set of animals, we used SNP analysis to estimate the percentage of C57BL/6 background, which was above 90% for all animals that were analyzed, indicating genetic background homogeneity.

Immunohistochemistry and histopathological analyses. Cryosections from perfused and PFA-fixed mid-cervical spinal cords were incubated in blocking solution and subsequently stained with antibodies against the following structures: phosphorylated neurofilaments (SMI 31, mouse IgG, 1:1,000; Covance), nonphosphorylated neurofilaments (SMI 32, mouse IgG, 1:1,000; Covance), glial fibrillary acidic protein (GFAP, chicken IgY, 1:500; Abcam ab4674), and hexokinase-1 (HK1, MAB1534, mouse IgG, 1:250, EMD Millipore). Alexa Fluor 488–coupled donkey antibodies recognizing mouse IgG (1:600, Dianova) were used as secondary antibodies. The sections were analyzed with an LSM 700 confocal microscope (Zeiss). For H&E, Luxol fast blue (LFB), and App stainings, spines were fixed, decalcified, dehydrated and cast in paraffin, and stained according to standard procedures of the UKE Mouse Pathology Facility. Primary antibodies against App (1:3,000, Millipore, MAB348) were visualized by the avidin-biotin technique with 3,3-diaminobenzidine. The slides were analyzed using a NanoZoomer 2.0-RS digital slide scanner and NDP.view2 software (Hamamatsu). Axonal counts from the dorsal columns, HK1, GFAP immunoreactivity, and App^+ axons within white matter were analyzed with ImageJ software (NIH), with fixed threshold intensities across experimental groups. Numbers of inflammatory foci per spinal cord cross-section (H&E) were quantified manually as previously described (4), and the area of demyelination as a percentage of the total analyzed area of white matter within a given LFB stained section was measured using NDP.view2 software (Hamamatsu).

T cell proliferation assay and flow cytometry of CNS-infiltrating immune cells. For analysis of T cell proliferation, lymph node and spleen cells from immunized mice were cultured in 96-well plates (Sarstedt) at 2×10^5 cells per well in complete mouse medium (RPMI 1640, 10% FCS, 50 μM 2-mercaptoethanol, 100 U/ml penicillin/streptomycin) and stimulated with $MOG_{35–55}$ peptide or anti-CD3 (145-2C11, 1:100; eBioscience). After 2 days, cells were pulsed with 1 μCi [methyl-^{3}H]thymidine (Amersham) per well for 16 hours. Cells were harvested and spotted on filter mats with a Harvester 96 MACH III M (Tomtec). Incorporated activity per well was assessed in counts per minute in a Beta counter (1450 Microbeta, Perkin-Elmer), and proliferation was calculated. For flow cytometric analyses, CNS-infiltrating cells were isolated by Percoll (GE Healthcare) gradient centrifugation 15 days after immunization, and total numbers of $CD45^+$ CNS-infiltrating leukocytes were quantified by using TruCOUNT beads (BD Biosciences). CNS-infiltrating leukocyte subsets were identified by staining with monoclonal antibodies to the following proteins in the presence of TruStain Fc receptor block (1:1,000, BioLegend): CD3e (1:100, PerCP-Cy5.5, BioLegend, clone 145-2C11), CD8a (1:300, APC, BioLegend, clone 53-6.7), CD11b (1:300, FITC, BioLegend, clone M1/70), CD11c (1:300, PE-Cy7, eBioscience, clone N418), CD45 (1:100, APC-Cy7, BioLegend, clone 30-F11), Ly6G (1:300, V450, BD Biosciences, clone 1A8), NK1.1 (1:50,

PE, eBioscience, clone PK136), and CD19 (1:100, BV510, BioLegend, clone 6D5). Immune cell populations from CNS-infiltrating cells were identified as previously described (4). All FACS data were acquired on a LSR II FACS analyzer (BD), and data analysis was performed with FlowJo vX analysis software (TreeStar).

Statistics. All values are expressed as mean ± SD or SEM. Where indicated, we analyzed for significance by using unpaired, 2-tailed Student's *t* test for two groups or 2-way analysis of variance with Sidak's or Fisher's post-hoc analysis for multiple comparisons as parametric tests. Mann-Whitney *U* test was used as a nonparametric test, when data did not show normal distribution. We considered $P < 0.05$ as significant and $P < 0.01$ as highly significant. Intraindividual variability was not considered; *P* values are exploratory. Data illustration and statistical analysis were performed using GraphPad Prism 6.

Study approval. All applicable international, national, and/or institutional guidelines for the care and use of animals were followed. All procedures were in accordance with the ethical standards of the German Animal Welfare Act. Ethical approvals were obtained from the State Authority of Hamburg, Germany (approval G13/022).

Author contributions

BS and WF designed the study, performed most of the experiments, and wrote the manuscript. BE generated transgenic mice. YL performed electrophysiology. BS, HL, DI, and MAF provided funding. HL, DI, and MAF supervised the project, designed experiments, and wrote the manuscript.

Acknowledgments

The study was supported by the Bundesministerium für Bildung und Forschung (DI, NGFNplus/EMINet project 01GS0831; HL, 01GS08123), the Deutsche Forschungsgemeinschaft (MAF, FR1720/9-1 within FOR2289; DI, IS63/3-1/2; HL, Le1030/10-2, Le1030/11-2), and the Novartis Pharma GmbH (BS, Oppenheim Förderpreis für Multiple Sklerose). This work benefited from data assembled by the ImmGen consortium. We thank J.B. Engler for ImmGen data visualization, S. Rosenkranz and the UKE Mouse Pathology Facility for help with experiments, H. Voss for animal caretaking, I. Hermans-Borgmeyer for ES cell culture, and R. Volland (Uniklinik Köln) for statistical advice.

Address correspondence to: Manuel A. Friese, Institut für Neuroimmunologie und Multiple Sklerose, Zentrum für Molekulare Neurobiologie Hamburg, Universitätsklinikum Hamburg-Eppendorf, Falkenried 94, 20251 Hamburg, Germany. Phone: 49.0.40.7410.56615; E-mail: manuel.friese@zmnh.uni-hamburg.de.

1. Dendrou CA, Fugger L, Friese MA. Immunopathology of multiple sclerosis. *Nat Rev Immunol*. 2015;15(9):545–558.
2. Friese MA, et al. Acid-sensing ion channel-1 contributes to axonal degeneration in autoimmune inflammation of the central nervous system. *Nat Med*. 2007;13(12):1483–1489.
3. Friese MA, Schattling B, Fugger L. Mechanisms of neurodegeneration and axonal dysfunction in multiple sclerosis. *Nat Rev Neurol*. 2014;10(4):225–238.
4. Schattling B, et al. TRPM4 cation channel mediates axonal and neuronal degeneration in experimental autoimmune encephalomyelitis and multiple sclerosis. *Nat Med*. 2012;18(12):1805–1811.
5. Kaplan MR, Cho MH, Ullian EM, Isom LL, Levinson SR, Barres BA. Differential control of clustering of the sodium channels Na(v)1.2 and Na(v)1.6 at developing CNS nodes of Ranvier. *Neuron*. 2001;30(1):105–119.
6. Craner MJ, Lo AC, Black JA, Waxman SG. Abnormal sodium channel distribution in optic nerve axons in a model of inflammatory demyelination. *Brain*. 2003;126(Pt 7):1552–1561.
7. Craner MJ, Newcombe J, Black JA, Hartle C, Cuzner ML, Waxman SG. Molecular changes in neurons in multiple sclerosis: altered axonal expression of Nav1.2 and Nav1.6 sodium channels and Na+/Ca2+ exchanger. *Proc Natl Acad Sci U S A*. 2004;101(21):8168–8173.
8. Foster RE, Whalen CC, Waxman SG. Reorganization of the axon membrane in demyelinated peripheral nerve fibers: morphological evidence. *Science*. 1980;210(4470):661–663.
9. England JD, Gamboni F, Levinson SR, Finger TE. Changed distribution of sodium channels along demyelinated axons. *Proc Natl Acad Sci U S A*. 1990;87(17):6777–6780.
10. Petracca M, Vancea RO, Fleysher L, Jonkman LE, Oesingmann N, Inglese M. Brain intra- and extracellular sodium concentration in multiple sclerosis: a 7 T MRI study. *Brain*. 2016;139(Pt 3):795–806.
11. Paling D, et al. Sodium accumulation is associated with disability and a progressive course in multiple sclerosis. *Brain*. 2013;136(Pt 7):2305–2317.
12. Bechtold DA, et al. Axonal protection achieved in a model of multiple sclerosis using lamotrigine. *J Neurol*. 2006;253(12):1542–1551.
13. Black JA, Liu S, Hains BC, Saab CY, Waxman SG. Long-term protection of central axons with phenytoin in monophasic and chronic-relapsing EAE. *Brain*. 2006;129(Pt 12):3196–3208.
14. Lo AC, Saab CY, Black JA, Waxman SG. Phenytoin protects spinal cord axons and preserves axonal conduction and neurologi-

cal function in a model of neuroinflammation in vivo. *J Neurophysiol*. 2003;90(5):3566–3571.
15. Black JA, Liu S, Carrithers M, Carrithers LM, Waxman SG. Exacerbation of experimental autoimmune encephalomyelitis after withdrawal of phenytoin and carbamazepine. *Ann Neurol*. 2007;62(1):21–33.
16. Craner MJ, et al. Sodium channels contribute to microglia/macrophage activation and function in EAE and MS. *Glia*. 2005;49(2):220–229.
17. Rush AM, Dib-Hajj SD, Waxman SG. Electrophysiological properties of two axonal sodium channels, Nav1.2 and Nav1.6, expressed in mouse spinal sensory neurones. *J Physiol (Lond)*. 2005;564(Pt 3):803–815.
18. Burgess DL, et al. Mutation of a new sodium channel gene, Scn8a, in the mouse mutant 'motor endplate disease'. *Nat Genet*. 1995;10(4):461–465.
19. Planells-Cases R, et al. Neuronal death and perinatal lethality in voltage-gated sodium channel alpha(II)-deficient mice. *Biophys J*. 2000;78(6):2878–2891.
20. Liao Y, et al. SCN2A mutation associated with neonatal epilepsy, late-onset episodic ataxia, myoclonus, and pain. *Neurology*. 2010;75(16):1454–1458.
21. Liao Y, et al. Molecular correlates of age-dependent seizures in an inherited neonatal-infantile epilepsy. *Brain*. 2010;133(Pt 5):1403–1414.
22. Lundgaard I, et al. Direct neuronal glucose uptake heralds activity-dependent increases in cerebral metabolism. *Nat Commun*. 2015;6:6807.
23. Bouafia A, et al. Axonal expression of sodium channels and neuropathology of the plaques in multiple sclerosis. *Neuropathol Appl Neurobiol*. 2014;40(5):579–590.
24. Waxman SG. Axonal conduction and injury in multiple sclerosis: the role of sodium channels. *Nat Rev Neurosci*. 2006;7(12):932–941.
25. Veeramah KR, et al. De novo pathogenic SCN8A mutation identified by whole-genome sequencing of a family quartet affected by infantile epileptic encephalopathy and SUDEP. *Am J Hum Genet*. 2012;90(3):502–510.
26. Jones JM, Meisler MH. Modeling human epilepsy by TALEN targeting of mouse sodium channel Scn8a. *Genesis*. 2014;52(2):141–148.
27. Wagnon JL, et al. Convulsive seizures and SUDEP in a mouse model of SCN8A epileptic encephalopathy. *Hum Mol Genet*. 2015;24(2):506–515.
28. Estacion M, et al. Ca2+ toxicity due to reverse Na+/Ca2+ exchange contributes to degeneration of neurites of DRG neurons induced by a neuropathy-associated Nav1.7 mutation. *J Neurophysiol*. 2015;114(3):1554–1564.
29. Ramien C, et al. Sex effects on inflammatory and neurodegenerative processes in multiple sclerosis. *Neurosci Biobehav Rev*. 2016;67:137–146.
30. Morsali D, et al. Safinamide and flecainide protect axons and reduce microglial activation in models of multiple sclerosis. *Brain*. 2013;136(Pt 4):1067–1082.
31. Black JA, Newcombe J, Waxman SG. Astrocytes within multiple sclerosis lesions upregulate sodium channel Nav1.5. *Brain*. 2010;133(Pt 3):835–846.
32. Pappalardo LW, Black JA, Waxman SG. Sodium channels in astroglia and microglia. *Glia*. 2016;64(10):1628–1645.
33. Black JA, Newcombe J, Trapp BD, Waxman SG. Sodium channel expression within chronic multiple sclerosis plaques. *J Neuropathol Exp Neurol*. 2007;66(9):828–837.
34. Black JA, Newcombe J, Waxman SG. Nav1.5 sodium channels in macrophages in multiple sclerosis lesions. *Mult Scler*. 2013;19(5):532–542.
35. Kapoor R, et al. Lamotrigine for neuroprotection in secondary progressive multiple sclerosis: a randomised, double-blind, placebo-controlled, parallel-group trial. *Lancet Neurol*. 2010;9(7):681–688.
36. Raftopoulos R, et al. Phenytoin for neuroprotection in patients with acute optic neuritis: a randomised, placebo-controlled, phase 2 trial. *Lancet Neurol*. 2016;15(3):259–269.
37. Waxman SG. Demyelination in spinal cord injury. *J Neurol Sci*. 1989;91(1-2):1–14.
38. Hains BC, Saab CY, Lo AC, Waxman SG. Sodium channel blockade with phenytoin protects spinal cord axons, enhances axonal conduction, and improves functional motor recovery after contusion SCI. *Exp Neurol*. 2004;188(2):365–377.
39. Eijkelkamp N, et al. Neurological perspectives on voltage-gated sodium channels. *Brain*. 2012;135(Pt 9):2585–2612.
40. Bosmans F, et al. Four novel tarantula toxins as selective modulators of voltage-gated sodium channel subtypes. *Mol Pharmacol*. 2006;69(2):419–429.
41. Bunting M, Bernstein KE, Greer JM, Capecchi MR, Thomas KR. Targeting genes for self-excision in the germ line. *Genes Dev*. 1999;13(12):1524–1528.
42. Hedrich UB, et al. Impaired action potential initiation in GABAergic interneurons causes hyperexcitable networks in an epileptic mouse model carrying a human Na(V)1.1 mutation. *J Neurosci*. 2014;34(45):14874–14889.